FEDERAL UNIVERSITY OF SANTA CATARINA
JOINVILLE TECHNOLOGICAL CENTER
MECHATRONICS ENGINEERING COURSE

LIGIA BENASSI YAMASHITA

AUTOMATED ADJUSTMENT OF A DUAL AXIS ACOUSTO-OPTIC DEFLECTOR

Joinville
2024

LIGIA BENASSI YAMASHITA

AUTOMATED ADJUSTMENT OF A DUAL AXIS ACOUSTO-OPTIC DEFLECTOR

This graduation thesis is presented to fulfill the partial requirement to obtain the title of bachelor in the course of Mechatronics Engineering, at the Joinville Technological Center, from the Federal University of Santa Catarina.

Supervising Professor: Prof. Dr. Tiago Vieira da Cunha

Co-Supervisor: Lucas de Andrade Both

Joinville
2024

I dedicate this work to my parents, both engineers, who always supported my academic ambitions.

ACKNOWLEDGEMENTS

I would like to thank the Fraunhofer Institute for Laser Technology ILT for allowing me to conduct this work in their facilities.
Furthermore, I would like to acknowledge Lucas de Andrade Both for his support as my co-supervisor, as well as Nicole Grubert and Tim Biermann for their help in the Fraunhofer facilities.
I am also forever grateful to my family and friends for the immense comfort and support throughout this journey, especially to my girlfriend, Simeia, who pushed me across the finish line.

We can easily forgive a child who is afraid of the dark; the real tragedy of life is when men are afraid of the light.
- Plato

ABSTRACT

Laser technology has become present in most significant industries of our modern society. The laser beam must be steered in order to be utilized appropriately, and the use of mechanical deflection technologies can provide sufficient range and working area for several fabrication processes, nevertheless, they cannot provide the necessary deflection speed and precision required for all processes. For applications requiring both a high angular range and deflection velocity, arranging a mechanical scanner and acousto-optic deflector (AOD) in series takes advantage of the most beneficial attributes of both components. The difficulty is utilizing an AOD is its dependency on the alignment of the incident angle to the so-called Bragg angle, which is hard to achieve and maintain manually in a system prone to vibrations and shifting. Therefore, this thesis presents the development of a system to achieve the Bragg angle at the entrance of an AOD. Its main objective is to automate the beam steering procedure using adjustable mirrors, optical sensors, and specialized control software.

Keywords: Acousto-optic deflector. Optical systems. Angular optical control. Diffraction efficiency.

RESUMO

Atualmente, lasers estão presentes nas áreas mais significativas da indústria e produção moderna. A orientação do curso de um laser é necessária para sua utilização apropriada, e através de tecnologias de deflexão mecânica é possível obter amplitudes e áreas de trabalho do laser suficientes para diversos processos de fabricação. No entanto, componentes mecânicos não podem fornecer a velocidade de deflexão e a precisão necessárias para todos os processos, sendo assim, para aplicações que necessitam alta amplitude angular e velocidade de deflexão, a utilização de um scanner mecânico e um defletor acústico-óptico (AOD) em série tira proveito dos atributos de ambos os componentes. No entanto, o funcionamento correto de um AOD é extremamente dependente do alinhamento do ângulo de incidência ao ângulo de Bragg, que deve ser alcançado de maneira precisa e mantido manualmente em sistemas sujeitos a vibrações e deslocamentos. Sendo assim, este trabalho apresenta o desenvolvimento de um sistema para obtenção do ângulo de Bragg na entrada de um AOD, que tem como objetivo a automação do processo de direcionamento de feixe do laser por meio de um sistema composto de espelhos ajustáveis, sensores ópticos e software de controle especializado.

Palavras-chave: Sistemas ópticos. Controle óptico angular. Eficiência de difração

LIST OF FIGURES

LIST OF TABLES

LIST OF ABBREVIATIONS AND ACRONYMS

ILT	Institut für Lasertechnik
AO	Acousto-optic
RF	Radiofrequency
AOD	Acousto-optic deflector

LIST OF SYMBOLS

λ	Optical wavelength
V	Velocity in the optical medium
v	Optical frequency
m	Diffraction order
Λ	Grating period/Acoustic frequency
TeO_2	Tellurium dioxide
M_2	Figure of merit
f_c	Central frequency
Δf	Frequency bandwidth
ω_m	Frequency of the mth order
n_m	Refractive index for the mth order
θ_B	Bragg angle

TABLE OF CONTENTS

1 INTRODUCTION

Since the first realization of a laser in 1960, applications for these devices have been investigated and are slowly evolving into market-relevant solutions. Presently, the technology has been applied in nearly all significant industries of our modern society, revolutionized several fields, and originated new research areas. It is clear that the world would not exist as it does today without lasers (SUGIOKA, 2021; AL-AMRI; EL-GOMATI; ZUBAIRY, 2016).

Industrial short and ultra-short pulse laser technology has advanced rapidly in recent years, offering new and powerful tools for surface structuring, cutting, and several other production processes (ZHONG; LONG, 2021). The use of ultra-short pulse laser systems as fabrication tools has been proven to provide high machining quality and negligible thermal effects for various materials, even at high processing speeds (MINCUZZI et al., 2018; STEIGER, 2018).

Despite the significant advances in laser processing techniques, some challenges remain. With growing demands from practical applications, standards are being increasingly raised on fabrication processes, aiming for more complicated architectures, smaller geometrical structuring, and higher productivity (FAN; ZHONG, 2021).

To fully exploit the capabilities of these ultra-short pulse laser sources in these applications, the beam deflection angle velocity must be in the order of thousands of radians per second. Unfortunately, the deflection angle velocities of frequently used servo-controlled mirror-based scanners are typically in the order of hundreds or fewer (RÖMER; BECHTOLD, 2014). Consequently, non-mechanical deflection technologies must be used to implement high-power and high-repetition-rate ultrashort pulsed lasers efficiently (BECHTOLD; HOHENSTEIN; SCHMIDT, 2013).

For applications requiring a high angular range and velocity, arranging a mechanical scanner and acousto-optic deflector (AOD) in series takes advantage of the most beneficial attributes of both components (RÖMER; BECHTOLD, 2014). In summary, an AOD consists of a crystal and a piezoelectric element; when an oscillating voltage is applied to the piezoelectric transducer, it converts the electrical energy into acoustic waves, that runs through the crystal and induces diffraction in the optical beam, steering its angle (ANTONOV; KOTELNIKOV, 2019).

The key attributes of AODs include their small size and weight, as well as their capacity to control laser radiation with a power density of up to hundreds of kW/cm^2 with a sufficiently high speed and minimal light losses, while not presenting the drawbacks of mechanical scanners, such as wear and tear, mechanical noise and drift. They can

also compensate vibrations and overshoots caused by fast mirror movements, reducing processing time and enhancing machining quality (FRANZ et al., 2022; ANTONOV; KOTELNIKOV, 2019; RÖMER; BECHTOLD, 2014).

Despite their many advantages over mechanical deflectors, in order to achieve the greatest possible diffraction efficiency with AODs, the incoming beam must hit the crystal at the so-called Bragg angle. Since the Bragg angle can be theoretically calculated, the main issue is constructing a setup capable of achieving this angle notwithstanding construction deviations and external disturbances. The high angular accuracy of AODs implies that the mechanical mounting of the device is the main cause of angular inaccuracies (BALAKSHY et al., 2021; RÖMER; BECHTOLD, 2014).

Given the many uses of AODs and their extreme dependency on the Bragg angle, this work aims to develop an automated system to achieve the Bragg angle. This will be achieved through the use of a set of electric actuated mirrors in order to steer the laser beam trajectory to the correct angle at the AOD entrance. Furthermore, a software interface to measure the power output laser beam using a power sensor and a control program will be developed to correct the orientation of the mirrors and adjust the laser input angle at the AOD.

1.1 OBJECTIVES

1.1.1 General objective

Development and construction of a system for the automated adjustment of an AOD at the Bragg angle, which later will be utilized in laser cutting functions at the Fraunhofer ILT.

1.1.2 Specific objectives

The specific objectives of this work are:

- Mount the electrical and mechanical test setup;
- Develop an interface with the driver of the kinematic mirror mounts and power sensor;
- Develop a control strategy and software for implementing such strategy;
- Develop software for data analysis and parameter optimization;
- Optimize the control algorithm based on the data analysis.

2 LITERATURE REVIEW

First, some concepts and technologies must be presented to comprehend better the contents discussed in this work and their relevance. A basis of optics and acousto-optics is established, and some physical phenomena and effects within these areas are explained in more detail, allowing for a better understanding of the principles behind acousto-optic deflectors and other components used in this work.

2.1 OPTICS

Optics is a branch of physics that focuses on studying light and other similar non-visible radiation. The exact nature of light is not completely known, but it is a form of radiant energy whose behavior can be described as a transversal wave motion. Therefore, equations such as Equation 1 can be used to describe light, with λ being the optical wavelength emitted by the source, V the velocity in the medium and v the optical frequency (FREEMAN; HASLER, 1990).

$$\lambda = \frac{V}{v} \tag{1}$$

2.1.1 Laser

When the light from a point source passes through a limiting aperture, a small group of rays called a pencil of light is formed. If the light source is larger than a point, we consider it to be comprised of several points, and the resulting collection of pencils is called a beam of light. From an ordinary light source, this wave motion is extremely complex as the motion comprises many waves in a random arrangement. The laser is a special source where the motion approaches that of a simple single wave (FREEMAN; HASLER, 1990).

The word laser was initially created as an acronym for "Light Amplification by Stimulated Emission of Radiation", and later developed into a word meaning the device for generating coherent electromagnetic waves by stimulated emission of radiation. Lasers can generate continuous waves or pulses with high directionality, completely controlled spatial and temporal phases, with varied frequencies and wavelengths. They are closest to a monochromatic light source currently (RENK, 2017; REIDER, 2016).

2.1.2 Diffraction

Keating (2002, p. 495) defines diffraction as the ability of waves to propagate around corners and obstacles. The effect occurs whenever a portion of a wavefront is

obstructed and is a general characteristic of wave phenomena, meaning that light waves are also capable of diffraction, although it is initially less evident due to their extremely short wavelengths. Recently, it has become possible to create optical elements with extremely fine embedded structures that interact with the wave nature of light and alter its direction; this is called a diffraction grating (HECHT, 2017; IIZUKA, 2019; FREEMAN; HASLER, 1990).

O'Shea et al. (2003) present the behavior of light regarding different obstacles, and with this, they prove that when a beam of light passes through any periodic structure within a medium, it is diffracted into multiple orders with angles depending on the wavelength of the incident beam. Considering a single medium (and therefore a constant velocity), Equation 1 shows that one frequency will directly correspond with one wavelength, and considering humans perceive different frequency ranges as a color spectrum, the diffraction grating can appear to separate light by its hue (HECHT, 2017).

Figure 1 – Diffraction of white light

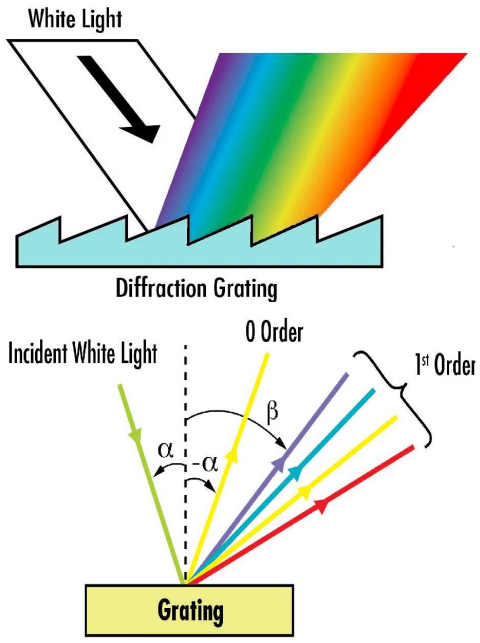

Source: adapted from Edmund Optics (2022).

Figure 1 shows the separation of the color spectrum resulting from the interaction between a diffraction grating and white light, composed of countless frequencies. If the incident light is monochromatic, such as light coming from laser sources, the grating will generate a group of regularly spaced beams or orders, whose direction is given by the grating equation, presented in Equation 2. In this equation, Λ represents the grating period, and θ_m the angle of the diffracted order m (O'SHEA et al., 2003, p. 83).

$$\sin \theta_m = \frac{m\lambda}{\Lambda} \tag{2}$$

2.2 ACOUSTO-OPTICS

The acousto-optic (AO) effect, also known as the elasto-optic effect, is defined as the change in the optical properties of a material due to strain. The interaction between a material and a propagating sound wave generates regions of rarefaction and compression, which induce a change in density, and a subsequent change in refractive index. This periodically changing refractive index acts like a diffraction grating moving at the speed of sound in the crystal (XU; STROUD, 1992; IIZUKA, 2019; RÖMER; BECHTOLD, 2014).

AO interactions can be either isotropic or anisotropic, depending on the optical properties of the crystal used as a medium. Any space through which light travels is considered an optical medium, most of which have the same properties in all directions and are, therefore, said to be isotropic. Materials that present different properties for different directions are called anisotropic; an example of a crystal commonly used in acousto-optics is paratellurite, the tetragonal crystal form of tellurium dioxide, or TeO_2 (IIZUKA, 2019; FREEMAN; HASLER, 1990).

2.2.1 Acousto-optic interactions

The interaction of acoustic and optical waves within a medium is the foundation of all AO systems; therefore, it is crucial to first comprehend the propagation rules of both acoustic and optical waves in media. An analysis of wave propagation involves two fundamentally different types of relationships: the first concerns universal laws, which are given by Maxwell's equations for optical waves and Newton's second law for acoustic waves; the second describes intrinsic properties of the medium, mainly the dielectric constitutive equation for optical waves and Hooke's law for acoustic waves(XU; STROUD, 1992).

The universal physical laws, when coupled with the equations that describe the properties of the medium, result in the fundamental equations governing wave propagation within anisotropic crystalline media. Due to the direction-dependent properties in anisotropic materials, these equation are usually expressed in tensor form. The equations defining the propagation of acoustic and optic waves are presented in full in Xu & Stroud (1992, p. 1-46) and in a more simplified version in Goutzoulis & Kludzin (1994, p. 1-24).

2.2.2 Diffraction regimes

Acousto-optic interactions are divided into two diffraction regimes, represented in Figure 2. The Raman-Nath regime is characterized by having multiple diffracted beams, also called diffraction orders, identified by the variable m.The Bragg regime

is characterized by showing a single diffraction order, where $m = 1$, as well as the undiffracted order, where $m = 0$ (GOUTZOULIS; KLUDZIN, 1994; CHANG, 1995).

Figure 2 – Diffraction modes. (a) Raman-Nath regime, (b) Bragg regime

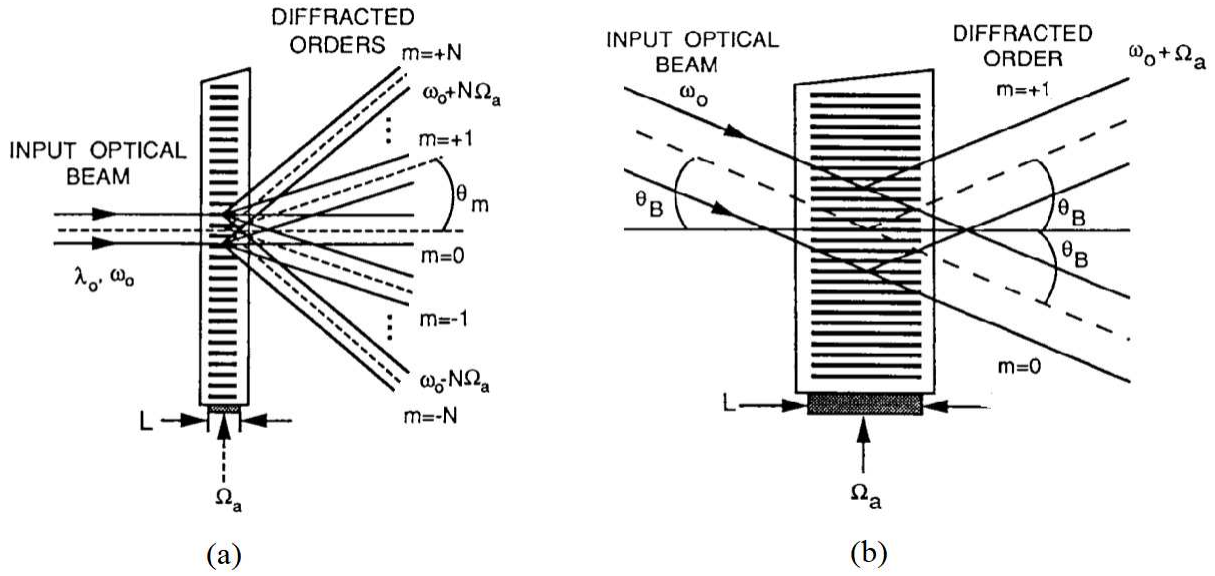

Source: adapted from Goutzoulis & Kludzin (1994).

The Bragg regime is achieved when the incident light enters the medium at the so-called Bragg angle, where only first-order refraction of the light is observed because higher-order diffraction beams undergo destructive interference. The Bragg angle is represented in Equation 3, derived from Equation 2 for the first order using the small angles sine approximation. The efficiency of converting the incident light to the diffracted order decreases dramatically if the direction of incidence strays from the Bragg angle, as the diffraction begins to exit the Bragg regime (RÖMER; BECHTOLD, 2014; IIZUKA, 2019).

$$\theta_B = \frac{\lambda_0 f_c}{2V} \tag{3}$$

Consequently, the Raman-Nath diffraction is not frequently used in practical devices due to its low diffraction efficiency, with its first order of diffracted light presenting approximately 34% intensity relative to the incident light. Bragg diffraction, on the other hand, is much more efficient, with the maximum obtainable diffraction efficiency being 100%, and therefore it is widely used in practical devices (CHANG, 1995; GOUTZOULIS; KLUDZIN, 1994).

2.2.3 Anisotropic AO interactions

Acousto-optic interactions that take place in anisotropic materials change the polarization of the optical beam and result in a single diffracted order. They offer

higher efficiency, as well as larger acoustic and optical bandwidths than the isotropic AO interactions; hence, most high-performance deflectors being based on anisotropic interactions. Aside from the actual AO interaction employed, the device performance also depends on the inherent properties of the AO material used, in almost all cases the requirements require high diffraction efficiency (GOUTZOULIS; KLUDZIN, 1994).

The figure of merit, represented by M_2, relates the diffraction efficiency to the acoustic power for a given material and device geometry. High-efficiency materials must have a high refractive index and a low acoustic velocity. A material with a large M_2 value is paratellurite, one of the most common mediums for modern AO devices. The crystal is transparent in a wide range of wavelengths, has a high radiation resistance and a well-developed technology of growth and processing. Furthermore, the theory for devices using these crystals is thoroughly described in the literature(GOUTZOULIS; KLUDZIN, 1994; TSAI, 1990; ANTONOV; KOTELNIKOV, 2019).

2.3 ACOUSTO-OPTIC DEVICES

The acousto-optic effect is generally implemented by attaching a suitable material to a piezoelectric transducer driven by a radio frequency (RF) source. As a response to the electrical frequency applied to the piezo, an acoustic wave is launched from the bottom of the cell containing the acousto-optic medium, and a periodic strain distribution is established. This strain distribution acts as a diffraction grating to any laser beam traveling through the material (IIZUKA, 2019; REIDER, 2016).

This implementation allows the traveling phase grating to deflect, modulate, or filter the optical beam. Devices based on these properties of the traveling phase grating are called acousto-optic deflectors, modulators, and tunable filters respectively. Although the underlying physical phenomena and acousto-optic interactions are the same, the design of these devices varies significantly (GOUTZOULIS; KLUDZIN, 1994).

2.3.1 Acousto-optic deflectors

The acousto-optic deflector (AOD) is a device capable of steering the diffraction angle of an optical beam by changing the frequency of the acoustic wave. Seeing as the Bragg diffraction is mostly used, the input laser beam must be fixed at the Bragg angle. The construction of this device will be expanded upon only as concerns Equation 3, where the relationship between the Bragg angle, the central frequency of the acoustic wave f_c, the input angle λ_0 and the velocity in the medium V is shown.

The angle of the diffracted beam is calculate by Equation 4, where $\Delta\alpha$ is the scanning angle and Δf is the frequency bandwidth; both properties determined by the construction of the AOD. Varying the acoustic frequency across the frequency bandwidth causes the deflected beam to cover its entire scan radius, where Δf denotes

the frequency bandwidth chosen such that the diffraction efficiency does not fall below 50% to 60%, (IIZUKA, 2019; RÖMER; BECHTOLD, 2014).

$$\theta_d(f) = \theta_B + \frac{\Delta\alpha}{\Delta f}(f - f_c) \tag{4}$$

2.3.2 Diffraction efficiency

The diffraction efficiency of an acousto-optic device pertains to the amount of light power transferred to the diffracted order beam from the input beam. This work mainly concerns how the diffraction efficiency relates to the input beam angle. Equation 5, from Tsai (1990)[p. 46] (originally derived by Gordon (1966)), shows the proportion of the light power of the diffracted order to the input light power as function of input angle and many other variables.

$$\frac{P_{\pm}(z)}{P_i(0)} = \frac{\pi^2}{2} M_2 \frac{L^2}{\lambda_o^2} \left(\sec\frac{\theta}{2}\right)^2 P_s \left[\frac{\sin\left(2\pi f_a L \Delta\theta/2\right)}{2\pi f_a L \Delta\theta/2}\right]^2 \tag{5}$$

Equation 5 can be simplified using the sine small angle approximation, assuming an input angle value close to the Bragg angle. However, even with the simplified equation, several values are reliant on construction details that are not revealed by most acousto-optic device manufacturers.

2.4 EXPERIMENTAL ANALYSIS

Scientific experimentation in conjunction with inductive inference allow new knowledge to be discovered. In experimentation, it is assumed valid inferences can be drawn from the data collected, that the particular cases chosen for experimentation are a good representation of the general case, and that a possible link will be established between cause and effect. Reaching any conclusion based on experimentation depends on the planning of tests followed by thorough documentation, analysis, and interpretation of the data obtained.

2.4.1 Design of Experiments

Fisher (1935) is a foundational work in the design of experiments. In this work, the author emphasizes the difficulty in determining which variables may affect the observed characteristics of a system when the relationships between the physical properties of said system are not fully known. The author also concurs with the importance of varying conditions one at a time, prevalent in scientific experimentation, while noting that the testing of different parameters in isolation disregards the possible interactions between them.

Factorial analysis is a tool for discovering the impact of different parameters on specific output characteristics by structuring tests based on all possible combinations of several values for each parameter. It is particularly useful for determining which parameters are most significantly affecting the output characteristics. When only one replication of each test is performed, it is not possible to estimate the interactions between different parameters; only the effects of variation among a single parameter may be investigated (LIPSON; SHETH, 1973).

2.4.2 Data analysis

Tukey (1977) first introduced the concept of the box-and-whisker plot, also known simply as box plot, as a tool for visualizing a batch of values. It is based on what Tukey calls the 5-value summary, where 5 values are used to summarize the general trend of the batch values. These are named the median, the hinges, and the extremes.

The median is the center value taken from an ordered list of all values in a batch, while the extremes are the lowest and highest values in a batch. The hinges, also known as quartiles, can be understood as the median of the subset of values between the actual median and each extreme, representing the value at 1/4th and 3/4ths of an ordered list of all values in a batch.

Figure 3 – Components of a box plot

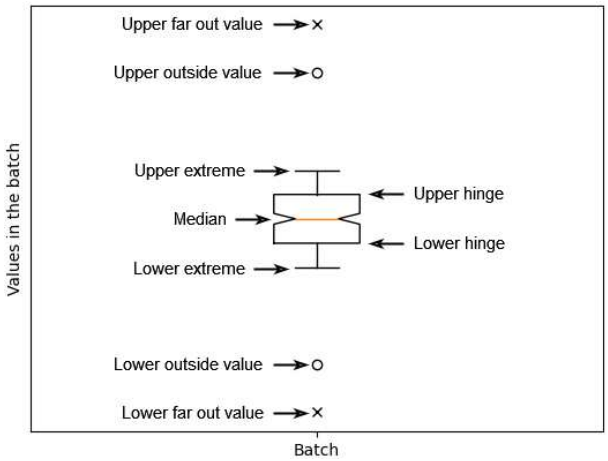

Source: elaborated by the author

The extremes are not good expressions of the batch values overall when their values are too distinct from the majority. In the interest of identifying these incongruous extremes, the concept of "outside"and "far-out"values is introduced. Another value is necessary to define these outliers, namely the "H-spread", also known as the interquartile range or IQR, which is the range between the two hinges that, when multiplied by 1.5, is called "step". Far-out values are those more than 2 steps from the hinge, and outside values are between 1 and 2 steps of the hinge.

The box plot is visually represented by a box ranging from the lower to the top hinges with a central line representing the median. The two whiskers extend to each direction until the most extreme (highest and lowest) values within the interval of 1 step. The outliers are represented as points with different symbols depending on whether they are an outside or far-out value. Figure 3 presents the components of the box plot.

The box plot is very useful for estimating a batch's characteristics visually. It can be constructed in other to visually evaluate whether a more in-depth analysis of the data may reveal a correlation, or if the discrepancies will be so minor as not to warrant further analysis.

3 METHODOLOGY

This chapter presents the methodology for the development of a system that automatically adjusts a laser beam to the Bragg Angle. First, all the components used are presented highlighting the characteristics that will be important for this work. The next section details the software that must be written for proper communication and control. In the end of the chapter, the test cases that will performed are displayed.

3.1 COMPONENTS

A test bench must be assembled in order to simulate and validate the adjustment system. In the tests, a laser will be steered by two piezo actuators attached to a kinematic mirror mount, which will alter the laser beam angle before entering an AOD through controls sent to the motor controller. The deflected laser beam exiting the AOD will reach an optical power sensor and the optical power meter will transfer the sensor data to a computer.

The components were all provided by the Fraunhofer-Intitut für Lasertechnik for the purpose of the development of this work and the test bench was constructed in a clean room in this institute.

3.1.1 Laser

The laser used in this work is the redEnergy G4 Fiber Laser produced by the company SPI Lasers (now rebranded to Trumpf), which will be used in continuous mode, generating a beam with a 3 mm diameter and a wavelength of 1064 nm. Given that the laser power should bear no influence in the system developed in this work, and with the aim of increasing safety during development and testing, the laser chosen had significantly lower power than those employed in production and cutting, reaching up to 60 W power and allowing the user to set a minimum of 10% of the maximum power.

Figure 4 – G4 Fiber Laser

Source: SPI Lasers, 2020.

3.1.2 AOD

The AOD used in this work is the DTSXY-400 2-axis acousto-optic deflector by AA Optoelectronics, presented in Figure 5. This device is designed to work with a single wavelength and, in the case of this work, the wavelength is 1064nm. Several properties of this AOD are listed in Table 1.

Figure 5 – DTSXY-400 2-axis Acousto-Optic Deflector by AA Optoelectronics

Source: AA Optoelectronics, 2022.

Table 1 – Constants for the DTSXY-400 AOD

Property	Symbol	Value	Unit
Figure of merit[1]	M_2	793×10^{-18}	s^3/g
Central frequency[2]	f_c	74	MHz
Frequency bandwidth[2]	Δf	30	MHz
Scan radius[2]	$\Delta\alpha$	49	$mrad^2$
Acoustic power[2]	P_a	2	W
Acoustic velocity[2]	V	650	m/s
Optical wavelength[2]	λ_0	1064	nm

Source: elaborated by the author

As explained in section 2.3.1, the AOD requires the adjustment of the incident optical beam to the Bragg angle in order to provide the highest possible diffraction efficiency. Figure 6 is the graph of the diffraction efficiency along the bandwidth of the frequency and it shows that, with the proper adjustment of the incident angle, diffraction efficiency can reach up to 80%.

[1] UCHIDA, N.; OHMACHI, Y. Elastic and photoelastic properties of TeO_2 single crystal. **Journal of Applied Physics**, v. 40, n. 12, p. 4692–4695, 1969.

[2] AA OPTOELECTRONICS. *DTSX - DTSXY*: Ao deflectors 1-axis/2-axis. Orsay, France, 2022. Available at: http://www.aaoptoelectronic.com/wp-content/uploads/2018/08/DTSxx-ed1-18.pdf. Access on: Oct. 14 2022.

Figure 6 – Diffraction efficiency vs. Driver Frequency

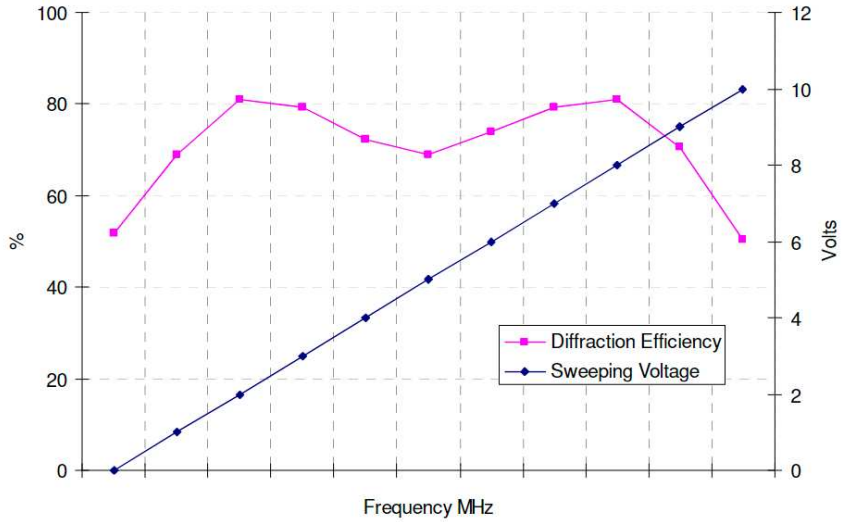

Source: Adapted from AA Optoelectronics, 2022.

3.1.3 Variable frequency drivers

In the test bench, each axis of the AOD is connected to a voltage controlled oscillator, particularly the DRFA variable frequency driver by the company AA Optoelectronics. This device responds to a variation in input voltage with a proportional change in output power amplifier, and this frequency signal must later go through an AMPB-B-34 power amplifier, also produced by AA Optoelectronics.

The driver is connected to 24 V power and has two connections whose voltage determines the amplitude and frequency, with the voltage input going from 0 to 10 V which has a linear correlation with a frequency from 50 to 110 MHz, meaning the output frequency can be determined by Equation 6.

$$f_{output} = 50 + 6U_{input} \tag{6}$$

Therefore, in order to achieve the AOD central frequency of 74 MHz, presented in Table 1, we must supply the frequency input with 4 V. In the system developed, the central frequency will be used and the amplitude input will be set at the maximum value of 5 V. The two amplifiers are connected to the two axes of the AOD, each with a fan on top of it to disperse the heat it generates; and both the amplifiers and fans should be connected to a 24 V power supply.

3.1.4 Kinematic mirror mounts

The mirror mounts used are the KM100 kinematic mirror mounts by Thorlabs, presented in Figure 7, which can hold mirrors with 1 inch of diameter and up to 3 mm of

thickness which are specific to the wavelength of 1064 nm. The mirror mounts are used to change the angle of the mirrors and consequently steer the laser beam.

Figure 7 – KM100 Kinematic Mirror Mount by Thorlabs

Source: Thorlabs, 2022.

This mount can rotate in two directions and the operation consists of the revolution of one of the screws in order to change the angle of the corresponding axes. This component provides an angular range of $\pm 4^o$ and a resolution of 8 mrad (approximately $0{,}46^o$) per turning of the screw in each of the axes.

3.1.5 Piezo inertia motor controller

The piezo inertia motor controller used in this work is the KIM101 by Thorlabs, presented in Figure 8. The function of this component in this work consists in sending power to the piezo inertial actuator, which will control the angle of the mirror mount and consequently steer the laser beam.

Figure 8 – KIM101 Piezo Inertia Motor Controller by Thorlabs

Source: Thorlabs (2022).

The programming libraries supplied by Thorlabs for communicating with this controller are compatible with many development tools, including C++. Through self-produced software it is possible to assign a value to one or more channels, that is, one

or more piezo actuator. The value set will be reached with incremental steps, and it is possible to define parameters such as the step rate and step acceleration.

3.1.6 Piezo inertial actuator

The piezo inertial actuators used in this work are the PIAK10 by Thorlabs, presented in Figure 9. The piezo inertial actuator is used for fine positioning and angular adjustment of the mirror mount. It maintains its position with no power applied and has an adjustment knob for manual positioning, making it suitable for the purposes of this work.

Figure 9 – PIAK10 Piezo Inertia Actuators by Thorlabs

Source: Thorlabs (2020).

For the use of the actuator in combination with KM100 mirror mount, the PIAK10 shows a typical angular resolution of 0,5μrad (approximately 28,65μ^o), meaning that 1 step of the driver pivots the mirror mount by 0,5μrad. Consequently, for the rotation of 1^o, approximately 34.904 steps are necessary; a value that will later be used as a multiplier in the inertial actuator control software.

This component utilizes a piezoelectric inertia "stick-and-slip"motor which rotates the screw, creating a proportional linear displacement of the corner of the mirror mount. Due to its open-loop nature, piezo hysteresis, component variance and environmental conditions, the step size may vary by over 20% and is not normally repeatable.

3.1.7 Photodiode power sensor

The power sensor used in this work is the S121C photodiode by Thorlabs, presented in Figure 10. The sensor is used for measuring the power of the diffracted laser beam exiting the AOD.

The silicon photodiode power head is designed for general-purpose optical power measurements and shows advantages in relation to thermal sensors, especially

Figure 10 – S121C Standard Photodiode Power Sensor

Source: Thorlabs, 2022.

regarding sensitivity, speed, stability, and drift. This component has a power range from 500 nW to 500 mW, resolution of 10 nW, response time below 1 μs, and linearity over several decades.

3.1.8 Optical power and energy meter

The optical power and energy meter is connected to the photodiode power sensor to interpret its measurements. This instrument is also connected to the computer through a USB cable for sending the sensor data and defining the parameters of the instrument.

Figure 11 – PM100D Optical Power and Energy Meter

Source: Thorlabs, 2022.

The PM100D optical power and energy meter by Thorlabs, shown in figure 11, will be used in this work. The PM100D is designed to measure the optical power of laser light or other monochromatic light sources and the energy of pulsed light sources. Since the laser used in the system is continuous, only measurements of power apply and, for an accurate measurement, it is fundamental to declare the beam diameter and wavelength.

3.2 SOFTWARE

Several C++ libraries must be developed for the test bench with the aim of being as reusable and easy-to-use as possible, given that this system will continue to be used in the Fraunhofer ILT. The code will make use of several external libraries provided by Thorlabs for communication with their drivers as well as the glog library, and be built using Bazel.

An interface must be developed for the PM100D and KIM101 components to facilitate communication, setting parameters, and reading data; as well as a library to log the data from the test into files, storing the information of time, position in the X and Y axes, and the light power readings. With the ability to log data, read sensors, and control the actuators, tests can be run to investigate the behavior of the system in order to help determine a control strategy.

After a control strategy has been determined, a library must be developed containing control routines that attempt to maximize the light power input by changing the output sent to the piezo actuator motors. For the analysis of the tests investigating the behavior of the system and the functionality of the control, the Python language will be utilized. The choice of this language was motivated by the extensive libraries of graph plotting and the author's previous familiarity.

3.2.1 External libraries

Bazel was chosen as the building tool for the software produced for this work. Bazel is a free open-source build and test software tool produced by Google that supports various platforms and languages, while also being fast and reliable, keeping caches of all previously done work and tracking changes to both file content and build commands, which minimizes rebuilding (GOOGLE, 2022b).

Similar to building tools like Make, Bazel builds software applications from source code using a set of rules. It has advantages like using a human-readable, high-level build language and the fact it operates on the concepts of libraries, binaries, scripts, and data sets, shielding the user from the complexity of writing individual calls to tools such as compilers and linkers. All of theses characteristics led to the choice of Bazel for this work.

Logging will be implemented in the software with the library glog to facilitate error tracking and recording of tests. Google Logging (glog) is a C++ library developed by Google that implements application-level logging. The library provides logging APIs based on C++-style streams and defines various helper macros that simplify many common logging tasks. With this library, it is possible to implement logging by severity level, conditional logging, personalized log message prefixes, conditional aborting of the program, and more (GOOGLE, 2022a).

For controlling and communicating with the components produced by Thorlabs, several libraries provided by the company are used, especially those related to KIM101 and PMD100D. Extensive documentation for these libraries is available in the product manuals and are written in C++, motivating the selection of this language for this system.

3.3 DESIGN OF TESTS

After the development of software for communication, control and logging, a series of tests will be conducted in order to produce data for the analysis of the best parameters for the control. Factorial tests will be used, which were explained previously in Section 2.4.1; with one test being performed for each combination of the parameters and their set of values, which are presented in Table 2. The definition of these parameters is presented in details in Section 4.4.

Table 2 – Control test conditions

Parameter	Abbreviation	Values			Unit
Tolerance	TOL	0.1	0.5	1	$\%$
Initial step size	ISS	$-$	500	1000	$step$
Precision step size	PSS	5	10	20	$step$
Initial step rate	ISR	$-$	1500	2000	$step/s$
Precision step rate	PSR	$-$	150	300	$step/s$
Approximate distance	DIS	200	1000	2000	$step$

Source: elaborated by the author

4 DEVELOPMENT

In this chapter, the development of the test bench will be presented, from the mechanical construction to software development and control strategies. After this, the results from tests performed in this test bench will be analyzed, ending in a discussion of the test results and limitations of this work as a whole.

4.1 TEST BENCH CONSTRUCTION

The test bench was organized to affix all components to the table surface with M6 screws, as shown in Figure 12, to ensure minimal movements and thus repeatability among the test cases. The AOD is mounted on a 4-axis stage which allows for 2 degrees of freedom for translation and 2 for rotation; and other components are attached to supports that allowed for rotation and changes in height. The components must be positioned in a way as to achieve an input beam angle as close as possible to the Bragg angle.

Figure 12 – Testing setup

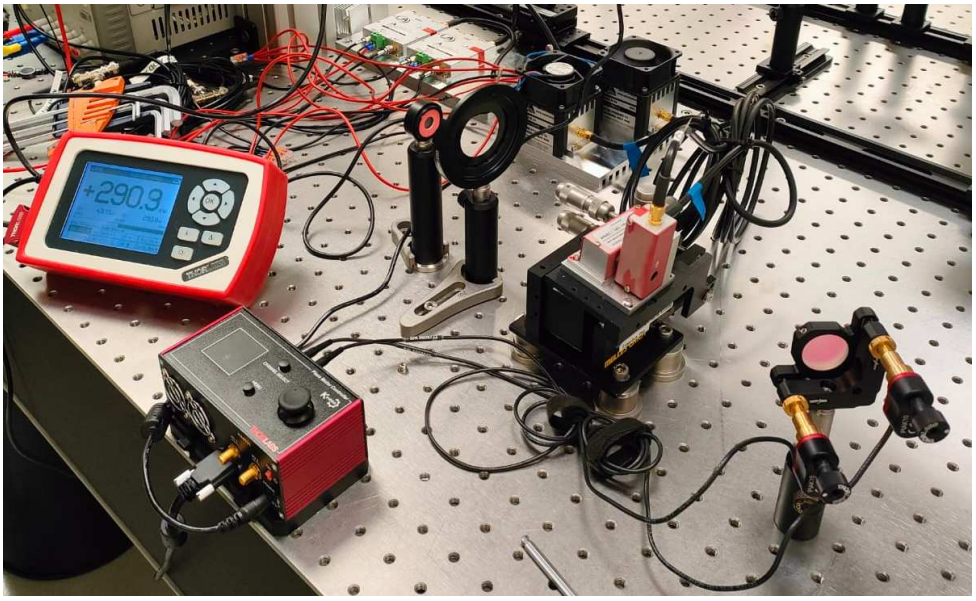

Source: elaborated by the author

In this system, the computer will read the measurements of the S120C sensor through the PM100D power meter, then, using the control software, an adequate response will be calculated and sent to the KIM101 driver, which will activate the two PIAK10 actuators, consequently changing the angle of the KM100 mirror mount and steering the laser beam. The operation of the testbench is illustrated in Figure 13.

Figure 13 – Operation diagram

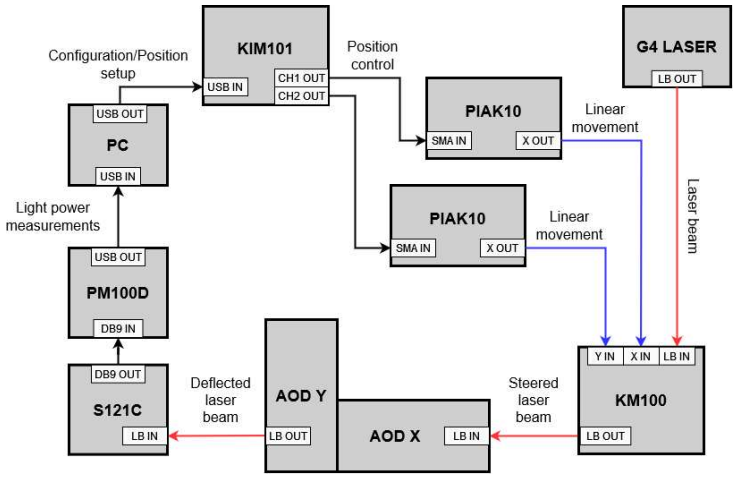

Source: elaborated by the author

The electrical properties of some of the components were already presented in Section 3.1, now the electrical setup of the entire system is presented in Figure 14. This figure displays the wiring and connections between components, as well as the power supply for them, with the direction of arrows indicating the flow of energy or information.

Figure 14 – Electrical setup and connections

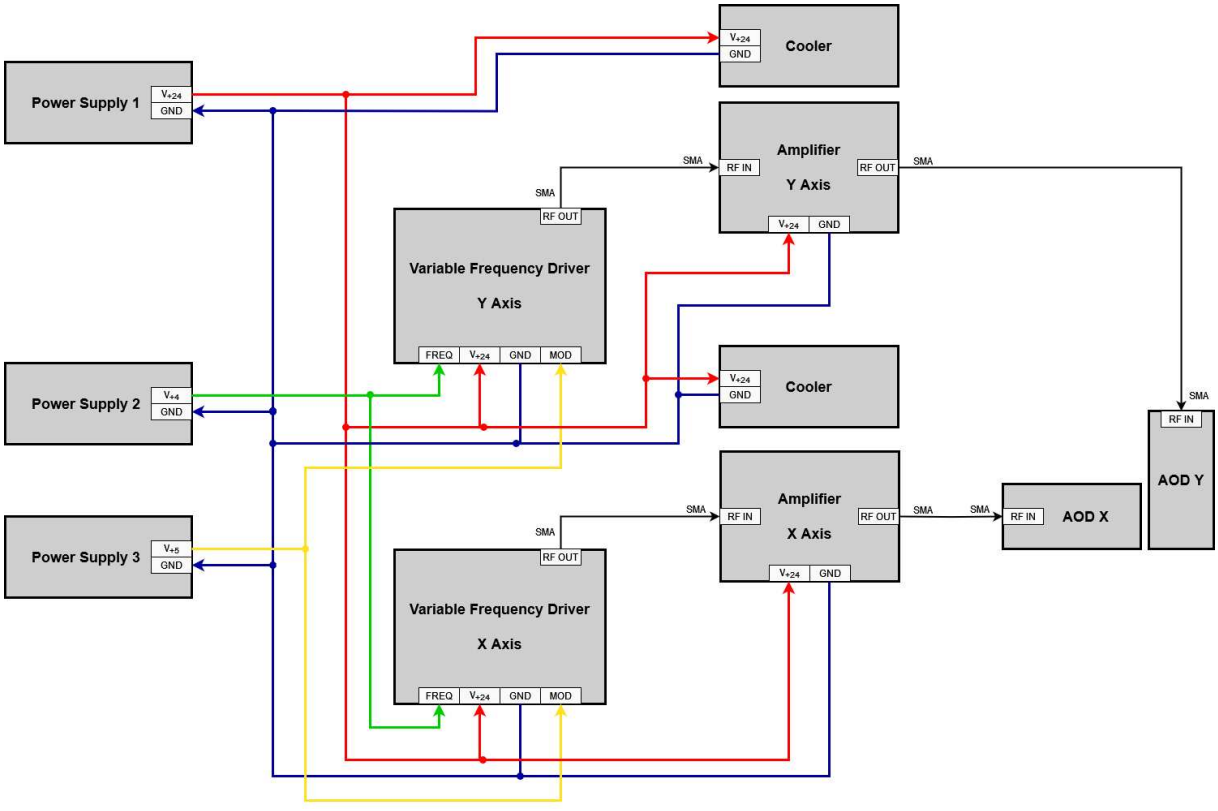

Source: elaborated by the author.

4.2 SOFTWARE

The initial step in developing the software was to map the necessary requirements for each of the libraries. The functional requirements for the software are listed in the items and more detailed requirements are listed in the subitems, with all the software being developed attempting to follow good practices of object-oriented programming while making easy-to-use and reusable software. In the end of the subsection for each library, the result of the development is summarized.

4.2.1 KIM101

The library implementing the communication with the piezo motor controller was named after the component code KIM101, the functional requirements for which were defined as follows:

F1 Connecting to the KIM101;
F2 Setting parameters such as: maximum voltage, step rate and step acceleration;
  F2.1 Ensuring the limits of all components are respected when setting these parameter;
F3 Sending messages to two different channels, for the control of the two axes;
  F3.1 Converting messages from physical angle of the mirror mount to steps of the controller;
F4 Reading from two different channels, regarding the position of the two axes;
  F4.1 Converting from steps read from the controller to the angle of the mirror mount;
F5 Logging information, warnings and errors in a log file;

Figure 15 – UML class diagram - KIM101

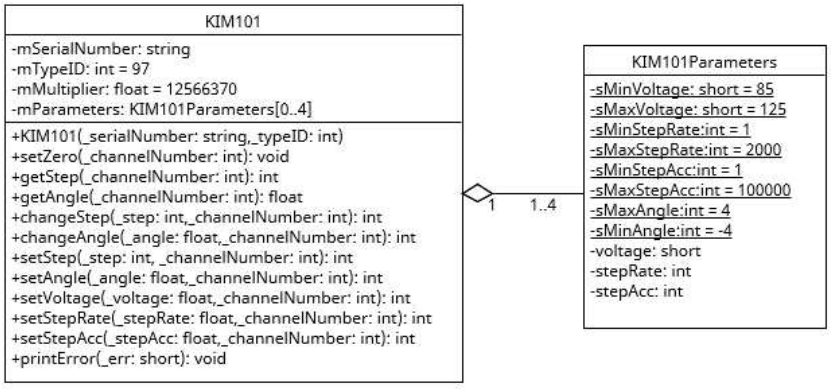

Source: elaborated by the author.

The library developed is represented by the UML class diagram in Figure 15, where the KIM101Parameters class was used to contain the static and non-static

characteristics of each of the channels used, where a channel is the connection between the controller and each piezo actuator.

The code developed was able to successfully interface with the piezo motor controller and move the two attached piezo actuators. This was validated through the available screen on the controller component, were the parameters displayed matched those send or read by the computer. The requirements were fulfilled with the exception of F3.1 and F4.1. The hysteresis of the actuators presented in Subsection 3.1.6 and the lack of a sensor for a feedback response impede the accurate conversion of steps to degrees.

4.2.2 PM100D

The library implementing the communication with the optical power and energy meter was named after the component code PM100D, the functional requirements for which were defined as follows:

F1 Connecting to the PM100D optical power and energy meter;
F2 Initializing the device;
F3 Setting the beam diameter according to the laser used;
F4 Setting the wavelength according to the laser used;
F5 Reading the information of light power from the S120C sensor;
F6 Performing multiple measurements to ensure accuracy;
F7 Logging information, warnings and errors in a log file;

The library developed is represented by the UML class diagram in Figure 16, utilizing variable types defined in the *visatype.c* file provided by Thorlabs, the manufacturer of the power meter.

Figure 16 – UML class diagram - PM100D

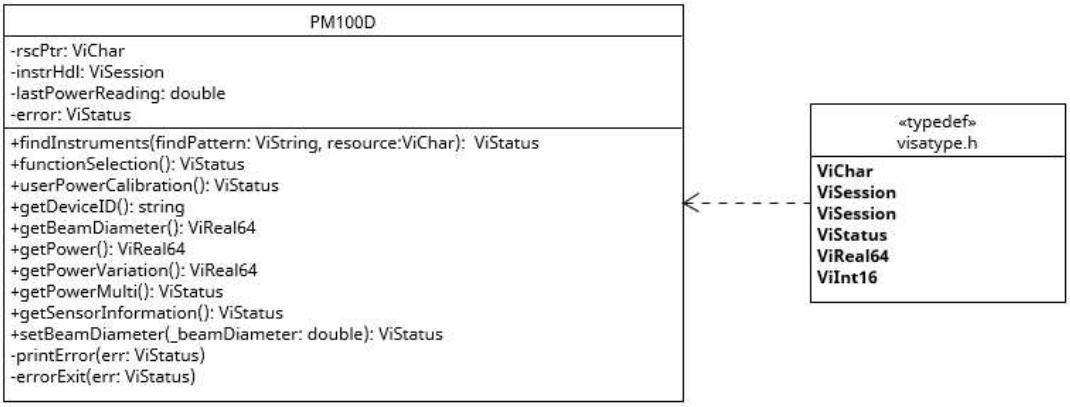

Source: elaborated by the author.

The code developed was able to successfully interface with the power meter

and the information read was consistent with what was displayed in the component's screen. Hence, the functional requirements for this library were considered to be fulfilled.

4.2.3 Test Log

The library developed for logging the data from tests performed was named TestLog, the functional requirements for which were defined as follows:

F1 Maintaining current time during tests;
F2 Saving information of time, light power, and the position in the X and Y axes during tests;
F3 Writing data to a CSV file after the end of a test;

Figure 17 – UML class diagram - TestLog

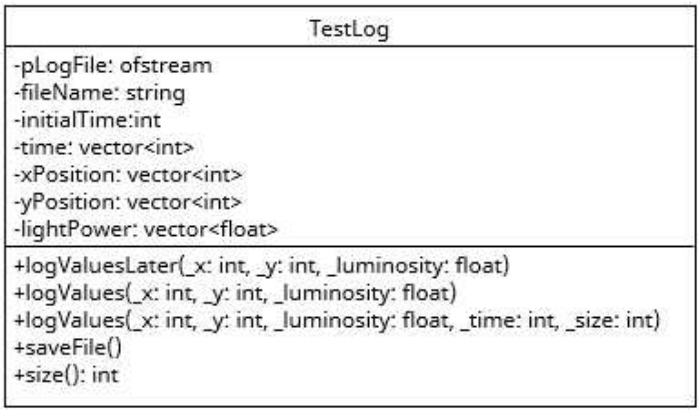

Source: elaborated by the author.

The library developed is represented by the UML class diagram in Figure 17. The initially developed function *logValues()* produced logs where the time intervals between each logged value were to large. The delay was assumed to result from the repeated access to the log file. Thus, the *logValuesLater()* function was written, where values were added to a vector of *int* variables, and only transferred to the log file at the end of the test.

4.2.4 AOD Control

The library developed for controlling the system to achieve maximum light power was named AOD control, the functional requirements for which were defined as follows:

F1 Connecting to the inertial motor and power sensor libraries;
F2 Controlling the inertial motor based on information read from the power sensor;
F3 Achieving the angle with maximum power output;
F4 Achieving the desired angle in an adequate amount of time;

F5 Logging the values of position, time, and light power;

Figure 18 – UML class diagram - AODControl

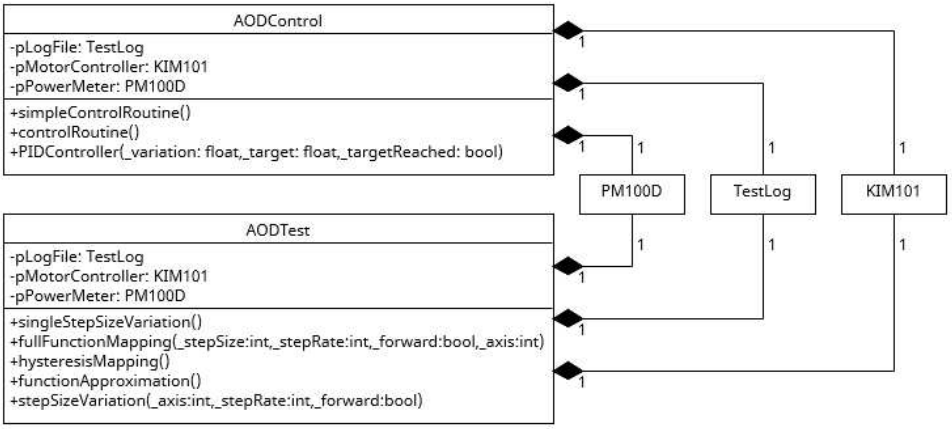

Source: elaborated by the author.

The library developed is represented by the UML class diagram in Figure 18, as well as its relationship with the previously presented classes. Within the library, a second class was created, named AODTest, composed of routines to investigate the behavior of the system, most of which will be presented further in this work. The fulfillment of the functional requirements of this library is dependent upon the validation of the system as a whole, and will be analysed in the remainder of this work.

4.2.5 Analysis

The functional requirements for the analysis software were defined as follows:

F1 Reading the CSV files of the tests;
F2 Separating the information of each column;
F3 Generating graphs;
F4 Comparing the data from several tests;
F5 Presenting graphs in the clearest and most concise manner possible;
F6 Generating graphs for several tests with minimal lines of command;

The library, developed in Python, has functions to open the CSV files and generate all graphs presented in the remainder of this work. Other functions separated the data by the value of one or more parameters, allowing for easier visualization and statistical analysis.

4.3 FUNCTION MODELLING

Several tests were run to empirically assess the behavior of the whole system, including the controller, piezo actuators, AOD, sensor and power meter; since all control

strategies must utilize these components and therefore should consider the possible errors inherent to them.

4.3.1 Equation fitting

For the purposes of this work, the most important physical property of the system is the relationship between the input angle of the light beam and the output light power. This function's shape was investigated by simply recording the output of light power while increasing steps of the piezo actuator linearly. This is shown in Figure 19, where the data was offset to align the highest value of light power with the origin of the angular position.

Figure 19 – Function shape

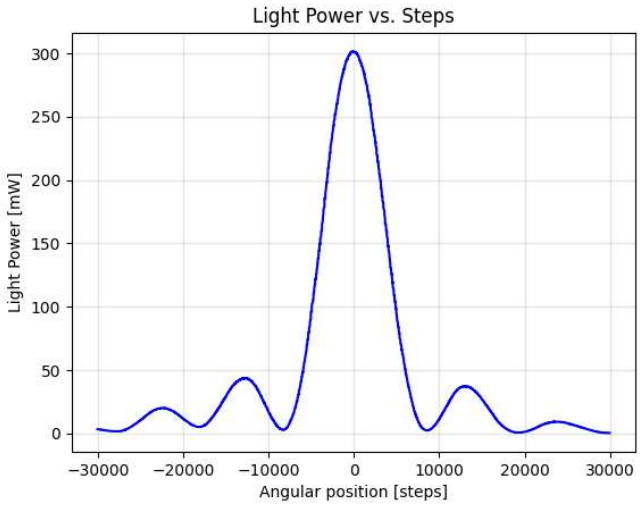

Source: elaborated by the author.

The profile present in Figure 19 seems similar to a function of $sinc^2(x)$, which is consistent with Equation 5. Further work would need to be done in order to fully describe light power as a function of input angle, such as converting the steps of the actuator to angle of the mirror and a validation of the value found for each constant based on the parameters Equation 5. However, as will be explained in Subsection 4.3.2, the description of this function in detail would not be of much help, and so no further efforts were put into modelling this function.

4.3.2 Hysteresis

When programming and testing the library for the KIM101 motor controller, the hysteresis of the piezo actuators controlling the mirror was noted to have a large effect in the consistency of the movement. In order to demonstrate the hysteresis visually, the

mirror was positioned manually to achieve a value close to the maximum, the controller then moved the mirror to the position of negative 10000 steps and positive 10000 steps, repeating this movement several times.

In the results, presented in Figure 20, the different colored lines each represent the power measurements of the sensor during one of direction of its movement. The legend shows the order of each of the paths and the sign shows whether the actuator was moving with positive or negative increments. Simply analyzing the data visually, it seems that while taking the same amount of steps, the negative direction does not return to the same position, with the decreasing steps seeming "shorter".

Figure 20 – Hysteresis test

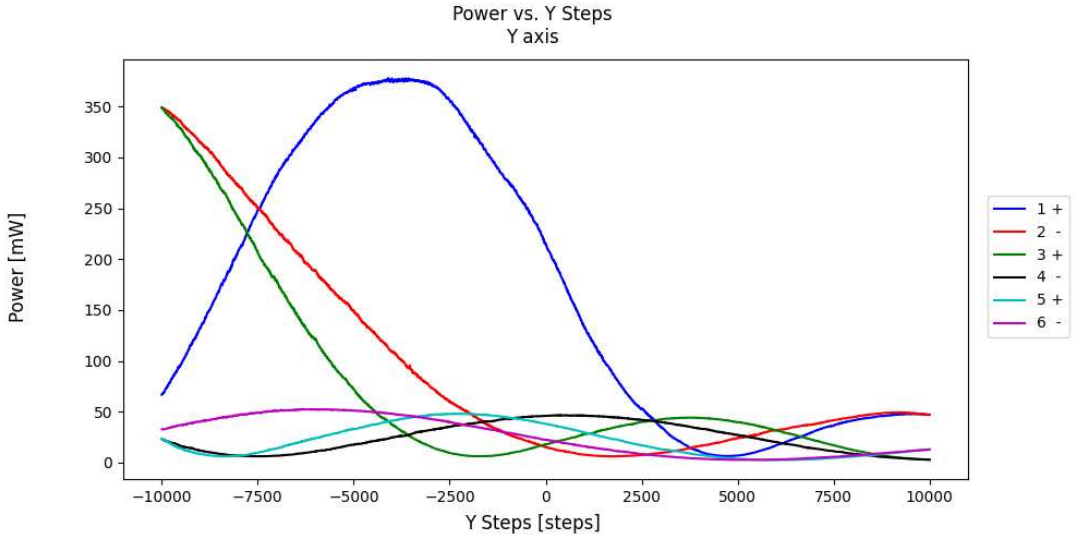

Source: elaborated by the author.

4.4 CONTROL STRATEGY

The initial plan for the control strategy was to use a well-known controller, namely the PID controller; however, this controller is used mostly to achieve a specific value in a system with a directly proportional relationship between input and output. Seeing as the aim of our system is to achieve a maximum value not yet known, and that the proportionality of the input and output is inverted after the peak, it was decided against the use of the PID controller.

The hysteresis of the actuator also complicates the correlation between the input (steps) and the output (light power), as it becomes dependent on the previous state of the system; this hinders the modeling of the function and development of a controller from this model. Works such as Abreu et al. (2023) show several techniques for modeling systems with hysteresis, however, the level of complexity this presents

goes beyond the scope of this work.

A new control routine was developed, the logic for which is represented in the activity diagram in Appendix A. When developing this logic, the parameters in Table 2 were selected as the most likely to affect the behavior of the system. The control strategy developed is quite useful due to the fact it does not require knowing the exact relationship between the angle and the light power, but as a trade-off, it must pass the peak once so that it may return, sacrificing some time.

4.5 CONTROL TEST RESULTS

Once a logic of control was established and the software developed, the control tests were performed to determine the best parameters for the system. The results of these tests were analyzed the final value of light power measured and the duration of the test.

Figure 21 – Overview of a regular test

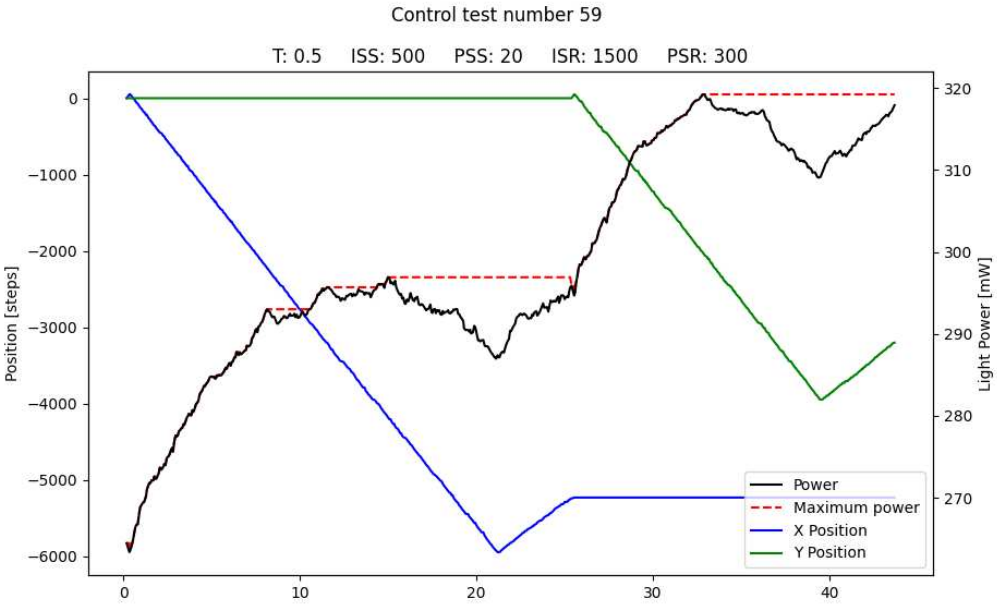

Source: elaborated by the author

Graphs were produced to visually represent each of the tests' runtime, with a regular test being presented in Figure 21. The parameters of the test are presented at the top of the figure below the title, following the abbreviations in Table 2. The red dotted line represents the current maximum value of light power found for the axis being adjusted, with the black line representing the light power measured at that time. The direction of movement is reversed once the measured power falls below a threshold, and continues in that direction until the measured light power falls until a tolerance of the maximum light power, as described in Appendix A.

A visual comparison was made among the test overview graphs, especially comparing those in which only one parameter value was altered. Aside from the change in slope of the axes' position lines, no striking differences were perceived in these comparisons. However, some tests were identified to have a peculiar repetition and a downward progression in the light power line.

Most tests performed presented a similar behavior to the test in Figure 21, presenting only one change in direction for each axis, disregarding the initial step to determine whether to increase or decrease the position; on the other hand, some tests presented a behavior more similar to Figure 22. Considering the relationship between the input angle and light power presented in Figure 19, it is reasonable to assume that the overall decrease in light power is due to outside influences unrelated to the control routine. Due to this decrease, tests such as the ones presented in Figure 22 display considerably longer total time.

Figure 22 – Overview of an inadequate test

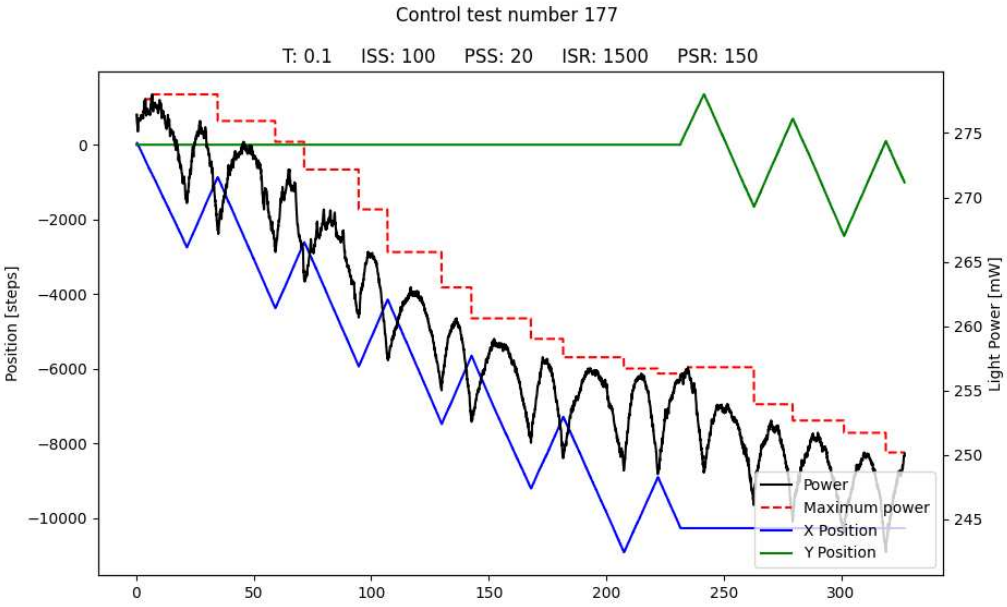

Source: elaborated by the author

Possible causes for this decrease are instability in the power supply or fluctuations in the light power output of the laser device itself, which became more apparent due to the use of lower power in the laser. Due to the assumption that this effect is unrelated to the variation in parameters and the ease of visually identifying tests in which this occurred, the choice was made to discard these results from the statistical analysis. This pattern of decrease, however, seems to not be completely unrelated to all of the parameters, as it was present in 8 of the 216 tests, all of which had a tolerance of 0.1%.

Box plots were generated through the analysis software developed, with the

intent of comparing the effects of the values of the parameters on the tests' duration and final light power achieved. As well as the visual analysis through the box plots, the test statistics were also assembled in Appendix B; where the mean, sample standard deviation and variance are presented in comparison for all values of each parameter as well as the statistics for all the tests, disregarding the 8 tests considered as inadequate. The values that presented the best results for each parameter were highlighted in gray.

While Appendix B provides a general idea of the influence of the parameter values, it consolidates tests performed at different distances, which disguises whether the performance of parameters is influenced by distance. Therefore, Appendix C presents the test statistics grouped by the approximate distance covered in the tests.

Figure 23 – Box plot of test time by levels of tolerance

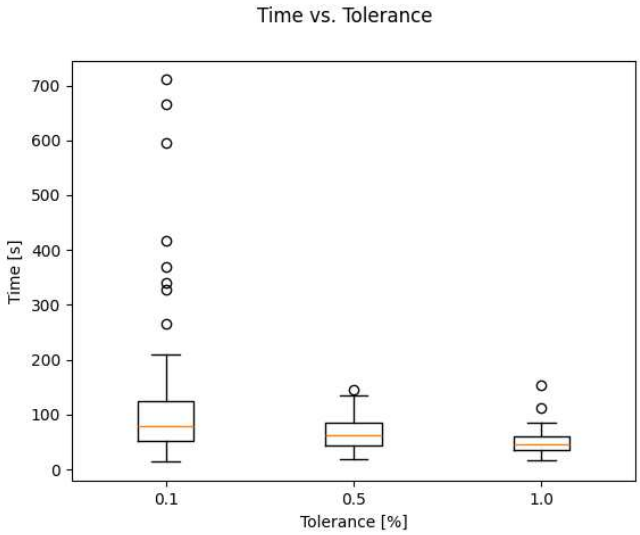

Source: elaborated by the author

Figure 23 is a box plot of the duration of tests separated by the tolerance percentage value without removing the tests previously identified as inadequate. The same 8 tests that presented visual irregularities also appear as outliers in the box plot. The medians for the tolerances of 0.1%, 0,5% and 1.0% were 77.866, 62.281 and 45.744 seconds respectively; however, the tolerance of 0.1% presented a standard deviation of nearly 5 times as large as the one for the other two tolerance levels.

After the removal of the outliers, the remaining tests where plotted for the analysis of the effects of all parameters and its values, which is presented in Figure 24. The most conspicuous correlations appear in the tolerance and distance plots. While the relationship between the distance and the elapsed test time is somewhat obvious, the trend in the time plot is relevant. The tolerance value of 0.1% still presented a higher median even after discarding the outliers, and the duration of test seems to be inversely related to the tolerance percentage value, which is also supported by Appendix B.

The duration column of the table in Appendix B shows which value achieved

Figure 24 – Box plot of time in relation to parameters

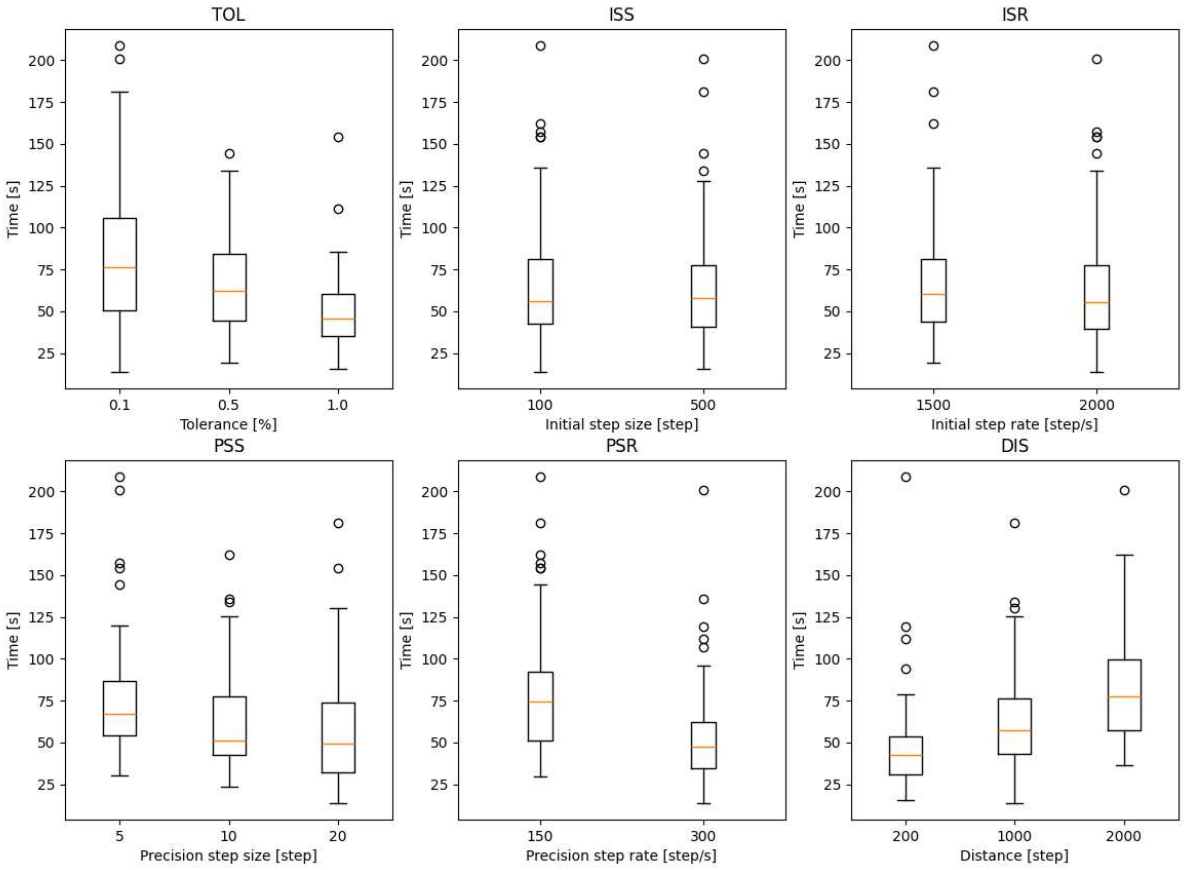

Source: elaborated by the author

a lower mean value of test duration, which is not as perceptible in the box plot. For all parameters used in these tests, disregarding distance, the highest value performed better in regards to duration. The data in Appendix C also seemingly supports this, with the few exceptions being values with higher standard deviation, suggesting irregularities in the tests' data.

The effect of parameters on the final light power achieved by the system is presented in Figure 25, with a box plot for each parameter. The different levels for most of the parameters present similar median values. Due to the speculated fluctuations in the laser light power seen in some tests it is difficult to affirm that the small differences in value seen in this graph are in fact related to the parameters.

Logically, the control routine should measure a higher light power for a smaller tolerance value, however, the data in Appendix B seems to contradict this, showing the shortest test duration for the tolerance of 0.5%. Examining Appendix C, the data for the best value of tolerance is inconclusive, varying with each distance. This inconsistency could be explained by accidental movements in the test setup between tests or variations in input light power; nonetheless it brings uncertainty to any inference drawn from the analysis of light power.

Figure 25 – Box plot of final light power in relation to parameters

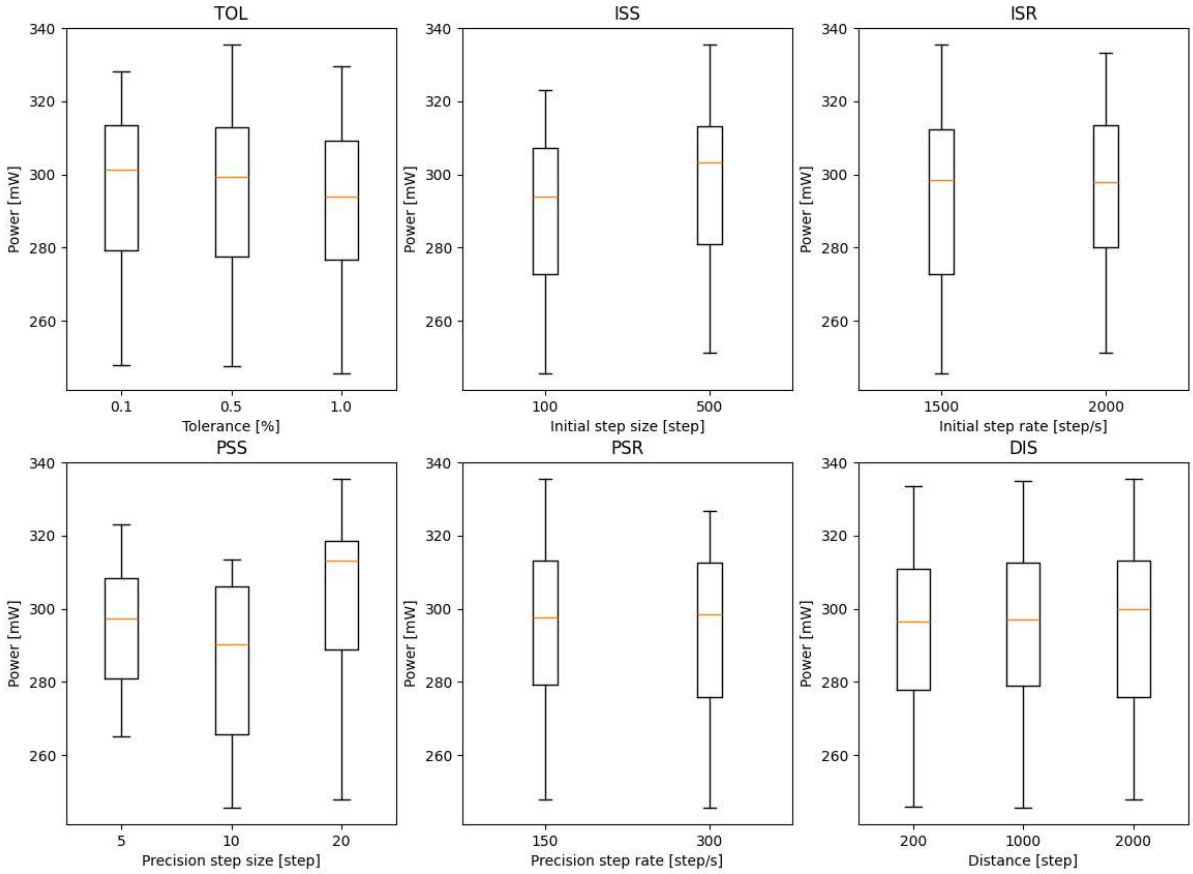

Source: elaborated by the author

4.6 DISCUSSION

Due to characteristics of the system observed in the attempt at modeling it, such as its function shape and inherent hysteresis, the PID controller was considered inadequate for the control. The aim of achieving a maximum value that was not previously known and was variable during the test would also complicate the implementation of this controller. The control routine developed seeks to account for the many outside factors and avoids many of the problems that hysteresis presents by dissociating input and output.

In the optimization of parameters, the tolerance of 0.1% was considered inadequate, seeing as 8 of the 72 tests with this level of tolerance presented a significantly larger duration, which could result in an unpredictable duration of the control routine. In the worst case, the test duration was nearly 10 times as long as the median for this tolerance value, which is far beyond an acceptable duration of time for an adjustment that must be performed regularly.

The parameters of step size and step rate were tested with multiple values, due to the concern of larger values resulting in high speeds that would miss the peaks of light power. This did not prove to be a problem in this system, likely due to the optical

response being nearly immediate when compared to the timescale of mechanical movements; and also possibly due to the small size of the individual steps allowed by the piezo actuator.

The data presented shows that, in regards to the duration of tests, all parameters exhibited a superior performance in their highest value. However, the analysis of light power was not as conclusive, with the seemingly arbitrary variation of power bringing uncertainty to any apparent correlation. Accordingly, the parameter values considered optimal were adopted from the duration analysis; that is, tolerance of 1%, initial step size of 500 steps, precision step size of 20 steps, initial step rate of 2000 steps/s and initial step rate of 300 steps/s.

4.7 LIMITATIONS

In this section, the limitations in the development and testing of this system will be addressed. Most limitations presented are a result of time constraints, as the laboratory used for the experiments was a shared space, with access restricted to specific times; and the experimental part of this work was produced over a limited period in a different country than that of the university.

The system developed requires an initial manual adjustment that must place the input beam in the central peak of the light power. Given the logic used for the control, if the system is placed incorrectly, it may only achieve a local maximum, which as shown in Figure 19, represents a significantly lower diffraction efficiency. The manual adjustment is a time-consuming process based on trial and error, meaning this system does not reduce as much setup time as expected.

The control software is also quite susceptible to external factors such as variations in input laser light power. Decreases in light power can drastically increase the duration of the control routine, while sudden increases in light power may result in the control routine concluding its execution without achieving the Bragg angle.

Ideally, multiple tests would be conducted with the same parameters and the mean value of these measurements would be utilized for the analysis, which was not possible in this work due to time constraints. With this larger batch size, a much more thorough statistical analysis could be conducted.

5 CONCLUSIONS

This work aimed to develop a system for the automated adjustment of the input angle of an AOD in order to allow for faster and easier tuning to the Bragg angle, which was previously performed manually at the Fraunhofer ILT. This was attempted by constructing a testing setup and conceptualizing a control strategy, which was later implemented into software, enabling several tests to be performed.

To achieve the main objective of developing and building a system for the automated adjustment of an AOD, five specific objectives were defined. The first specific objective, the mounting of the electrical and mechanical parts of the test setup, was achieved. The electrical connections allowed for all components to function in the testing setup, and the mechanical mounting required little to no changes after the setup, allowing for repeatability among tests.

The second and third specific objectives, the development of software for communicating with components and control software to achieve maximum light power, were also achieved. All pieces of software developed were able to fulfill its requirements, and the logic of control implemented was able to steer the angle to the maximum value found (within a tolerance) within the proposed span of time.

As for the last two specific objectives, due to time constraints, it was not possible to validate the chosen test parameter values, as the testing setup constructed was no longer accessible after the analysis of the test results was done. Nevertheless, the software for data analysis was produced and the plots it generated were instrumental in the decision of the final parameter values to be used in the control software.

5.1 SUGGESTIONS FOR FUTURE WORKS

Future works on this topic could be improved by performing tests with the same parameters multiple times and utilizing the mean value, making the results less susceptible to external effects, as removing an invalid test would not have such a great effect on the overall analysis and every possible combination of parameters values could be thoroughly analyzed. The validation of the control software with the chosen test parameter values is also an important step for any subsequent works.

To expand upon the present research, a more thorough investigation into the control of systems with hysteresis and into the modeling of diffraction efficiency as a function of input angle may be conducted. Such studies might reveal new control strategies that prove to be more efficient than the control software implemented in this work, maybe going so far as to waive the necessity of the initial manual adjustment of the input angle.

REFERENCES

AA OPTOELECTRONICS. *DTSX - DTSXY*: Ao deflectors 1-axis/2-axis. Orsay, France, 2022. Available at: http://www.aaoptoelectronic.com/wp-content/uploads/2018/08/DTSxx-ed1-18.pdf. Access on: Oct. 14 2022.

ABREU, P. et al. Identification and control of systems with hysteresis: concepts and tools. **International Journal of Modelling, Identification and Control**, Inderscience Enterprises, 2023.

AL-AMRI, M. D.; EL-GOMATI, M.; ZUBAIRY, M. S. **Optics in Our Time**. Cham, Switzerland: Springer Nature, 2016.

ANTONOV, S. N.; KOTELNIKOV, V. A. A review of physical principles and applications of acousto-optic deflectors on the basis paratellurite. **Physics & Astronomy International Journal**, v. 3, n. 6, p. 235–249, 2019.

BALAKSHY, V. et al. Acousto-optic cells with phased-array transducers and their application in systems of optical information processing. **Materials**, Mdpi, BASEL, v. 14, n. 2, p. 1–12, 2021.

BECHTOLD, P.; HOHENSTEIN, R.; SCHMIDT, M. Evaluation of disparate laser beam deflection technologies by means of number and rate of resolvable spots. **Opt. Lett.**, v. 38, n. 16, p. 2934–2937, aug 2013.

CHANG, I. C. Acousto-optic devices and applications: Devices, measurements, & properties. In: BASS, M. (Ed.). **Handbook of Optics**. 2. ed. New York, USA: McGraw-Hill, 1995. v. 2, cap. 12. (Optical Enginering, 41).

Edmund Optics. **All About Diffraction Gratings**. 2022. Available at: https://www.edmundoptics.eu/knowledge-center/application-notes/optics/all-about-diffraction-gratings/. Access on: Dec. 28 2022.

FAN, P.; ZHONG, M. Laser surface micro-nano structuring via hybrid process. In: SUGIOKA, K. (Ed.). **Handbook of Laser Micro- and Nano-Engineering**. 4. ed. Cham, Switzerland: Springer Nature, 2021. cap. 24.

FISHER, R. **The Design of Experiments**. Oliver and Boyd, 1935. (The Design of Experiments). Disponível em: https://books.google.com.br/books?id=-EsNAQAAIAAJ.

FRANZ, D. et al. Characterization of a hybrid scanning system comprising acousto-optical deflectors and galvanometer scanners. **Applied Physics B**, v. 128, n. 3, p. 1–9, feb 2022.

FREEMAN, M. H.; HASLER, B. L. **Optics**. 10. ed. Bodmin, England: Hartnolls, 1990.

GOOGLE. **Google Logging Library**. 2022. Available at: https://github.com/google/glog. Access on: Oct. 28 2022.

GOOGLE. **Intro to Bazel**. 2022. Available at: https://bazel.build/about/intro. Access on: Oct. 28 2022.

GORDON, E. I. A review of acoustooptical deflection and modulation devices. **Applied Optics**, Optica Publishing Group, v. 5, n. 10, p. 1629–1639, Oct 1966.

GOUTZOULIS, A. P.; KLUDZIN, V. V. Principles of acousto-optics. In: GOUTZOULIS, A. P.; PAPE, D. R. (Ed.). **Design and Fabrication of Acousto-Optic Devices**. New York, USA: Marcel Dekker Inc., 1994. cap. 1. (Optical Enginering, 41).

HECHT, E. **Optics**. 5. ed. Essex, England: Pearson Education, 2017.

IIZUKA, K. **Engineering Optics**. 4. ed. Cham, Switzerland: Springer Nature, 2019. 435-443 p.

KEATING, M. P. Chapter 22 - diffraction. In: KEATING, M. P. (Ed.). **Geometric, Physical, and Visual Optics**. 2. ed. Burlington: Butterworth-Heinemann, 2002. p. 495–521.

LIPSON, C.; SHETH, N. **Statistical Design and Analysis of Engineering Experiments**. McGraw-Hill, 1973. ISBN 9780070379916. Disponível em: https://books.google.com.br/books?id=D2wvvgAACAAJ.

MINCUZZI, G. et al. New fast galvo scanner head for high throughput micromachining. In: **Proceedings of SPIE - The International Society for Optical Engineering**. [S.l.]: SPIE, 2018. v. 10520, p. 105200X–105200X–7.

O'SHEA, D. C. et al. **Diffractive Optics: Design, Fabrication, and Test**. Bellingham, USA: SPIE Press, 2003.

REIDER, G. **Photonics**: An introduction. Cham, Switzerland: Springer International Publishing, 2016. 403-410 p.

RENK, K. **Basics of Laser Physics**: For students of science and engineering. 2. ed. New York, USA: Springer International Publishing, 2017.

RÖMER, G.; BECHTOLD, P. Electro-optic and acousto-optic laser beam scanners. **Physics Procedia**, Elsevier B.V, v. 56, n. C, p. 29–39, 2014.

STEIGER, E. New connecting and micro material processing techniques with ultra-short pulse lasers and high speed optical manufacturing tools. In: IVANOV, A.; BICKER, M.; PATZELT, P. (Ed.). **Tagungsband 1. Symposium Elektronik und Systemintegration ESI 2018: „Von der Sensorik bis zur Aktorik in interdisziplinärer Anwendung"**. [S.l.: s.n.], 2018. p. 17 – 25.

SUGIOKA, K. **Handbook of Laser Micro- and Nano-Engineering**. 4. ed. Cham, Switzerland: Springer Nature, 2021.

THORLABS. **PIA Series Piezo Inertia Actuators**: User guide. Ely, United Kingdom, 2020. Available at: https://www.thorlabs.com/drawings/70ede7b6bd30b6eb-66C7B4F9-BEA4-AC20-9B6294CC19BB5671/PIAK10-Manual.pdf. Access on: Oct. 14 2022.

THORLABS. **KIM101 Piezo Inertia Motor Controller**: Kinesis user guide. Ely, United Kingdom, 2022. Available at: https://www.thorlabs.com/drawings/70ede7b6bd30b6eb-66C7B4F9-BEA4-AC20-9B6294CC19BB5671/KIM101-KinesisManual.pdf. Access on: Oct. 14 2022.

TSAI, C. S. **Guided-Wave Acousto-Optics**: Interactions, devices and applications. Heidelberg, Germany: Springer-Verlag, 1990. (Springer Series in Electronics and Photonics, 23).

TUKEY, J. **Exploratory Data Analysis**. [S.l.]: Addison-Wesley Publishing Company, 1977. (Addison-Wesley series in behavioral science, v. 2). ISBN 9780201076165.

UCHIDA, N.; OHMACHI, Y. Elastic and photoelastic properties of TeO_2 single crystal. **Journal of Applied Physics**, v. 40, n. 12, p. 4692–4695, 1969.

XU, J.; STROUD, R. **Acousto-Optic Devices**: Principles, design and applications. New York, USA: John Wiley & Sons Inc., 1992. (Wiley Series in Pure and Applied Optics).

ZHONG, M.; LONG, J. Laser surface structuring of metals and functionalization. In: SUGIOKA, K. (Ed.). **Handbook of Laser Micro- and Nano-Engineering**. 4. ed. Cham, Switzerland: Springer Nature, 2021. cap. 25.

APPENDIX A - CONTROL ACTIVITY UML CHART

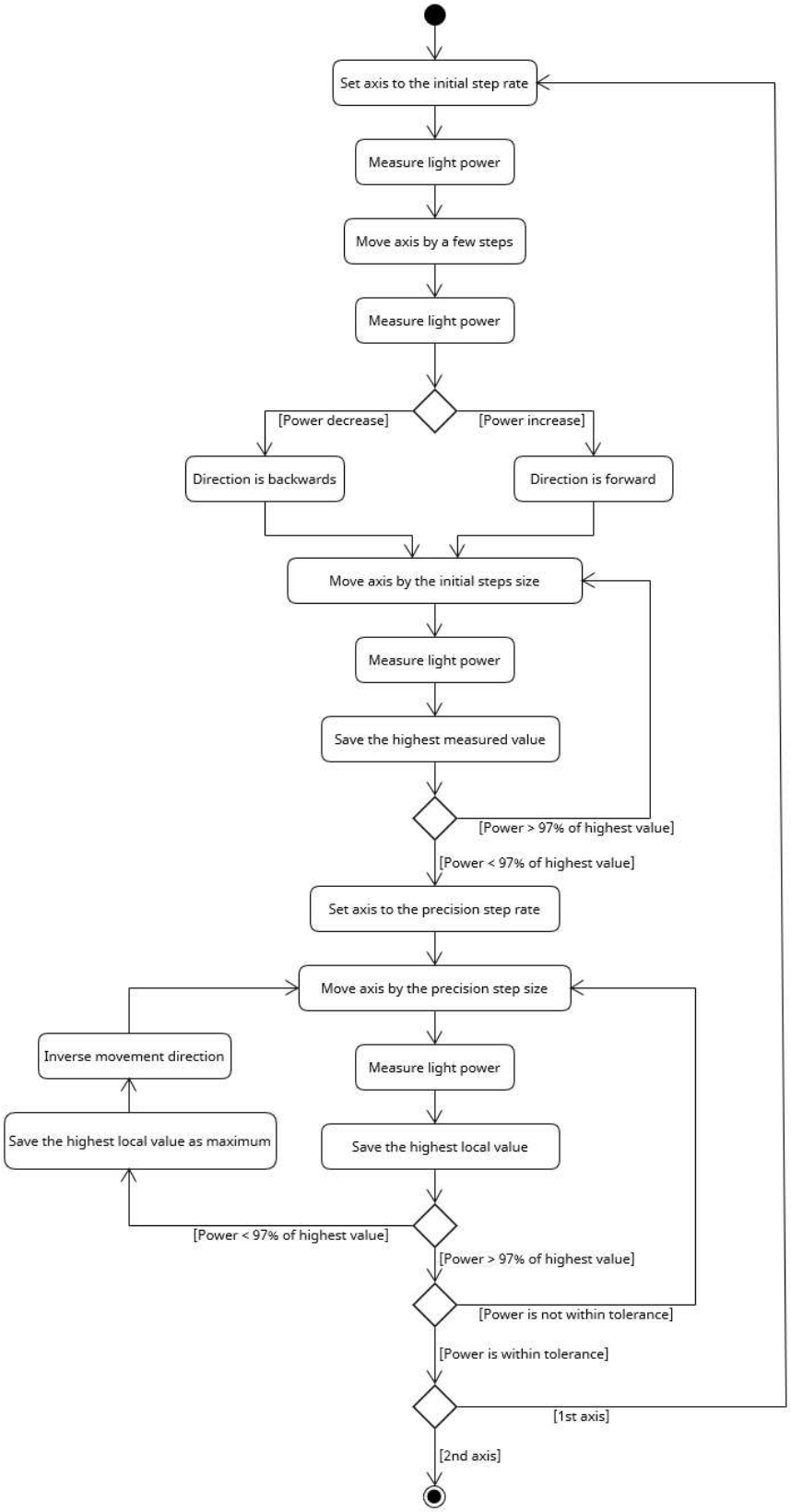

APPENDIX B - STATISTICS

		Duration [s]			Light power [mW]		
		Mean	Std. dev.	Variance	Mean	Std. dev.	Variance
Tolerance	0.1	82.756	43.060	1854.145	295.607	22.357	499.852
	0.5	65.198	27.440	752.977	296.871	21.346	455.656
	1.0	50.258	22.258	495.434	291.258	21.638	468.184
Initial step size	100	66.584	35.527	1262.144	289.651	22.257	495.359
	500	64.242	32.842	1078.613	299.548	20.204	408.187
Precision step size	5	75.947	35.742	1277.528	294.701	16.043	257.378
	10	62.288	29.406	864.743	284.369	23.284	542.160
	20	57.993	34.955	1221.841	304.809	20.620	425.176
Initial step rate	1500	66.816	33.999	1155.905	292.485	24.431	596.893
	2000	64.003	34.449	1186.762	296.631	18.574	345.004
Precision step rate	150	78.608	34.807	1211.542	295.560	21.704	471.079
	300	51.865	27.698	767.168	293.465	21.934	481.110
Approx. distance	200	48.173	28.905	835.477	294.060	21.695	470.671
	1000	63.638	29.503	870.435	294.186	22.022	484.969
	2000	83.741	34.397	1183.164	295.318	21.941	481.418
All tests		65.430	34.167	1167.411	294.527	21.790	474.813

APPENDIX C - STATISTICS BY DISTANCE

Distance			Tolerance			Initial step size		Precision step size		
			0.1	0.5	1.0	500	1000	5	10	20
200	Duration	Mean	63.380	47.589	36.718	51.100	45.158	66.628	41.807	35.246
		Std. dev.	42.581	22.331	12.306	35.836	19.503	38.481	14.339	16.684
		Variance	1813.162	498.690	151.442	1284.199	380.367	1480.774	205.615	278.356
	Power	Mean	298.931	295.244	289.019	289.055	299.217	293.163	283.301	305.757
		Std. dev.	21.348	21.668	21.837	22.378	20.007	16.520	24.190	18.511
		Variance	455.750	469.490	476.872	500.778	400.297	272.921	585.173	342.652
1000	Duration	Mean	77.160	67.364	47.516	61.309	66.103	66.157	65.254	59.431
		Std. dev.	37.557	25.019	15.389	25.804	33.191	20.101	29.087	37.596
		Variance	1410.526	625.958	236.840	665.832	1101.637	404.049	846.055	1413.452
	Power	Mean	293.950	297.629	290.958	289.703	298.932	294.779	284.404	303.800
		Std. dev.	23.321	20.964	22.260	22.577	20.695	16.463	23.755	21.417
		Variance	543.864	439.498	495.534	509.719	428.277	271.047	564.303	458.672
2000	Duration	Mean	104.116	81.313	66.541	87.052	80.429	95.057	78.097	78.313
		Std. dev.	40.585	24.600	25.793	35.047	33.915	38.615	29.820	33.025
		Variance	1647.180	605.189	665.301	1228.319	1150.224	1491.113	889.237	1090.638
	Power	Mean	294.445	297.777	293.798	290.178	300.458	296.162	285.314	304.912
		Std. dev.	22.877	22.252	21.466	22.446	20.464	15.711	22.932	22.519
		Variance	523.375	495.137	460.804	503.812	418.786	246.851	525.865	507.129

Initial step rate		Precision step rate		All tests
1500	2000	150	300	
53.223	42.970	54.061	42.107	48.173
34.710	20.633	30.490	26.262	28.904
1204.791	425.719	929.667	689.679	835.476
291.233	296.973	294.438	293.670	294.060
23.842	19.166	21.832	21.884	21.695
568.418	367.334	476.644	478.910	470.671
64.585	62.691	79.998	47.277	63.638
32.198	26.980	29.525	18.539	29.503
1036.706	727.920	871.709	343.688	870.435
292.286	296.086	295.753	292.619	294.185
25.114	18.603	22.047	22.205	22.022
630.699	346.070	486.068	493.078	484.969
81.826	85.768	100.440	66.059	83.741
29.588	39.206	28.269	31.622	34.397
875.467	1537.124	799.131	1000.004	1183.164
293.862	296.860	296.433	294.137	295.318
24.930	18.511	21.821	22.3339	21.941
621.497	342.675	476.148	498.803	481.418